



**HAL**  
open science

# In One Fell Sweep: Modeling Exchange, Hyperfine and Dipolar Interactions from EPR Spectra of Copper(II) Spin Triangles

Athanassios K Boudalis

► **To cite this version:**

Athanassios K Boudalis. In One Fell Sweep: Modeling Exchange, Hyperfine and Dipolar Interactions from EPR Spectra of Copper(II) Spin Triangles. *Magnetochemistry*, 2023, 9 (10), pp.217. 10.3390/magnetochemistry9100217 . hal-04280342

**HAL Id: hal-04280342**

**<https://hal.science/hal-04280342v1>**

Submitted on 10 Nov 2023

**HAL** is a multi-disciplinary open access archive for the deposit and dissemination of scientific research documents, whether they are published or not. The documents may come from teaching and research institutions in France or abroad, or from public or private research centers.

L'archive ouverte pluridisciplinaire **HAL**, est destinée au dépôt et à la diffusion de documents scientifiques de niveau recherche, publiés ou non, émanant des établissements d'enseignement et de recherche français ou étrangers, des laboratoires publics ou privés.

---

# In one fell sweep: modeling exchange, hyperfine and dipolar interactions from EPR spectra of copper(II) spin triangles

Athanassios K. Boudalis

Institut de Chimie de Strasbourg (UMR 7177, CNRS-Unistra), Université de Strasbourg, 4 rue Blaise Pascal, CS 90032, F-67081 Strasbourg, France. Email: bountalis@unistra.fr

Dedicated to Dr. Romain Ruppert on the occasion of his retirement.

**Abstract:** The weak intramolecular magnetic interactions within a series of  $\text{Cu}^{\text{II}}_3$  complexes based on the trinucleating 2,4,6-tris(di-2-pyridylamino)-1,3,5-triazine (dipyatriz) ligand were investigated by EPR spectroscopy. X- and Q-band EPR spectroscopy in powders and frozen solutions were recorded and the Q-band spectra were interpreted by a multispin Hamiltonian model comprising exchange, dipolar and hyperfine interactions. The described methodology is suitable for the elucidation of weak intramolecular interactions which are not amenable to analysis by SQUID magnetometry.

**Keywords:** EPR spectroscopy; spin triangles; dipolar interactions; hyperfine interactions; spin Hamiltonian

---

## 1. Introduction

Spin triangles constitute a “rediscovered” class of metal complexes,[1] whose magnetic properties have rendered them interesting as potential magnetoelectric materials,[2–6] with a proposed use as electrically controlled and slow-decoherence spin-chirality qubits.[7–10]

Our overall ability to design and implement such devices is predicated on our precise understanding of their magnetic structures, down to the finest details. Traditionally, the general strategy implemented to tackle this task is the same as with most other molecular magnetic materials: magnetometric techniques (e.g. SQUID magnetometry) are first used to elucidate the gross magnetic structure governed by isotropic (Heisenberg-Dirac-van Vleck) interactions and eventually antisymmetric (Dzyaloshinskii-Moriya) interactions, both of superexchange origins. Finer terms, such as zero-field splittings (zfs) or anisotropic interactions, are not very reliably assessed by magnetometric techniques, necessitating the use of spectroscopic techniques, the most prominent of which is Electron Paramagnetic Resonance (EPR) spectroscopy.

The use of EPR spectroscopy has its own limitations, e.g. when dealing with non-Kramers systems and very big zfs terms. While these systems are addressable by High-Frequency (W-band frequencies and above) or THz EPR, the availability of such experiments can be a limiting factor to their use. Classical EPR, however, i.e. at Q-band frequencies and below, can yield very precise information on weaker terms, such as hyperfine interactions. In addition, low-temperature studies can yield very informative data on the ground states of polynuclear complexes, which then can be used to verify the magnetometry-derived conclusions regarding exchange interactions.[11]

The above strategy works very nicely in cases where  $J \gg k_B T$ , A, i.e. at the strong exchange limit. When, however, exchange interactions are very weak with respect to the thermal energy and comparable to eventual hyperfine interactions, errors in magnetometric techniques (weighing, diamagnetic corrections) render their use problematic. The large diamagnetic content of biological magnetic systems, can give rise to such problems even for strong exchange interactions. In such cases, EPR spectroscopy can often yield useful information. However, a careful construction of the model is then required, to include any term that might influence the EPR spectrum. These include not just isotropic interactions, but also the full description of the system symmetry that influences its anisotropic terms. These may include Dzyaloshinskii-Moriya interactions (DMI), dipolar interactions, anisotropic exchange and hyperfine interactions, taking proper care to model the various tensor orientations (e.g. **g**, **A**, etc) and vectors connecting the different spins.

In previous work we showed that it is possible to derive very accurate descriptions of the magnetic properties of trinuclear  $\text{Cu}^{\text{II}}$  complexes [12] by properly accounting for the dipolar terms which induce a zfs in their quartet states. Such studies are not only applicable on single-crystal data, but also to those from randomly oriented samples (powders or frozen solutions). In those previous cases, hyperfine interactions were not considered, either because they were unresolved, or because they were very weak, respectively. Moreover, it was considered that their inclusion might render the problem computationally intractable; in the case of  $\text{Cu}^{\text{II}}_3$ , the Hilbert space would reach a dimension of  $(2S + 1)^n \times (2I + 1)^m = 512$  for  $S = 1/2$  ( $\text{Cu}^{\text{II}}$ ),  $I = 3/2$  (for  $^{63/65}\text{Cu}$ ), and for  $n = m = 3$  electron and nuclear spins, further complicated by the need to calculate  $2^3 = 8$  possible isotopologues for the  $^{63/65}\text{Cu}$  nuclei.

---

The renewed interest of spin triangles as spin-chirality qubits involves excitation of the “chiral transitions” *between*, not within, the low-lying spin doublets. Therefore, engineering the interdoubt energy gap  $\Delta$  becomes a question of interest. For spin triangles with monatomic bridges (e.g.  $\text{O}^{2-}$ ,  $\text{OH}^-$ ,  $\text{RO}^-$ ) this can be in the order of  $\sim 10^2 \text{ cm}^{-1}$  for  $\text{Cu}^{\text{II}}_3$  triangles,  $\sim 10^1 \text{ cm}^{-1}$  for  $\text{Fe}^{\text{III}}_3$  triangles and  $\sim 10^0 \text{ cm}^{-1}$  for  $\text{Cr}^{\text{III}}_3$  triangles, i.e. in the THz and FIR regimes. Large trinucleating ligands in place of monatomic ones impose larger interspin separations, allowing us to eventually modulate this energy and lower it within the GHz regime, which is more tractable by EPR instrumentation.

Ligand 2,4,6-tris(di-2-pyridylamino)-1,3,5-triazine (dipyatriz), has in the past been used to construct such molecular architectures. Its attractiveness in copper(II) chemistry lies in the fact that the axial ligands of copper(II) ions can be easily changed by proper choice of synthetic conditions, namely the relative ratios of  $\text{CuCl}_2 \cdot 2\text{H}_2\text{O}$  and  $\text{Cu}(\text{ClO}_4) \cdot 6\text{H}_2\text{O}$  starting materials. Exchanging neutral for anionic ligands can therefore be used to rationally modify the total charge of the molecule. Indeed, previously reported complexes include  $[\text{Cu}_3(\text{dipyatriz})_2\text{Cl}_3](\text{ClO}_4)_3$  (**1**) [13],  $[\text{Cu}_3(\text{dipyatriz})_2(\text{H}_2\text{O})\text{Cl}_2](\text{ClO}_4)_4$  (**2**) [13],  $[\text{Cu}_3(\text{dipyatriz})_2(\text{H}_2\text{O})_3](\text{ClO}_4)_6$  (**3**) [14],  $[\text{Cu}_3(\text{dipyatriz})_2\text{Cl}_3][\text{CuCl}_4]\text{Cl}$  (**4**) [15] and  $[\text{Cu}_3(\text{dipyatriz})_2\text{Cl}_3]\text{Cl}_3$  (**5**) [16], with electric charges of the molecules rationally modifiable from +3 to +6 without noticeably changing the structure of the metal core (though the +5 complex  $[\text{Cu}_3(\text{dipyatriz})_2(\text{H}_2\text{O})_2\text{Cl}](\text{ClO}_4)_5$  has not yet been reported, its synthesis should in principle be feasible through modification of the molecular ratios of  $\text{CuCl}_2 \cdot 2\text{H}_2\text{O}$  and  $\text{Cu}(\text{ClO}_4) \cdot 6\text{H}_2\text{O}$  used for the new synthesis of complex **2** reported here). This feature constitutes a degree of freedom for the control of solubilities in desired solvents.

This was therefore deemed a suitable system to construct spin triangles characterized by moderate to weak interactions, and use EPR spectroscopy to assess their magnetic structures far more accurately than it is possible with magnetometric techniques.

This work describes the modeling of the spin Hamiltonian parameters of a series of  $\text{Cu}^{\text{II}}_3$  spin triangles of similar structures (Figure 1) using continuous-wave (CW) EPR data at the X- and Q-bands. From a general perspective, these results outline a methodology to fully account for features of EPR spectra arising from exchange and dipolar interactions, by accurately describing the spatial arrangement of the tensorial and vectorial terms of the multispin Hamiltonian. Moreover, the specific results provide precise estimates of exchange interactions mediated by an extended organic superexchange pathway. Such precise estimates, quite difficult to come by via magnetometric methods, are valuable for the calibration of theoretical methods attempting to derive such exchange terms from first principles.

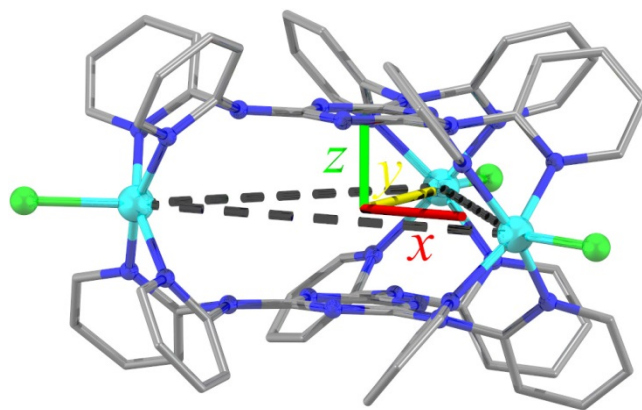


**Figure 1.** POV-Ray plot of the cation of **1** superposed to the molecular reference frame  $R_M$  used in the analysis of its magnetic properties. This is a right-handed reference frame with its origin  $O$  at the center of an idealised equilateral triangle, with  $x \parallel r_{12}$ , and  $z$  normal to the triangle plane.

## 2. Results

In the original work [13] no magnetic studies were reported for **1**. For the structurally related complex **4**, SQUID magnetometry yielded antiferromagnetic interactions ( $J = +0.42 \text{ cm}^{-1}$ ) with  $g_{\text{iso}} = 2.04$ ; these results, however, needed to also account for the Curie contribution of the  $[\text{CuCl}_4]^{2-}$  counteranion putting the derived values into question due to possible correlations.[15] In related work, SQUID magnetometry of **3** also yielded AF interactions, though much weaker, i.e.  $J = 0.08 \text{ cm}^{-1}$  ( $g_{\text{iso}} = 2.07$ ).[14]

Preliminary EPR studies at the X- and Q-bands in the solid state (Figure 2) revealed largely unresolved spectra for **1** and **2**. These exhibit clear low-field features which disappear upon dissolution. Thus, these might tentatively be attributed to half-field and third-field transitions due to intermolecular dipolar interactions. However, the complexity of simulating EPR spectral features stemming from intermolecular interactions precludes their confident assignment.

On the other hand, a fine and hyperfine structure are observed in the spectra of **3** both in the X- and the Q-bands. At the same time, the low-field region (not shown) is completely devoid of any features. The factors influ-

encing EPR spectra in the solid state are more complicated due to the extended intermolecular interactions, but a plausible explanation for the above observations is that the larger intermolecular distances between the hexacations of **3**, must play a role in reducing dipolar broadenings in the solid state. Indeed, the shortest intermolecular Cu...Cu distances are 7.262, 8.829 and 9.686 Å for **1**, **2** and **3**, respectively.

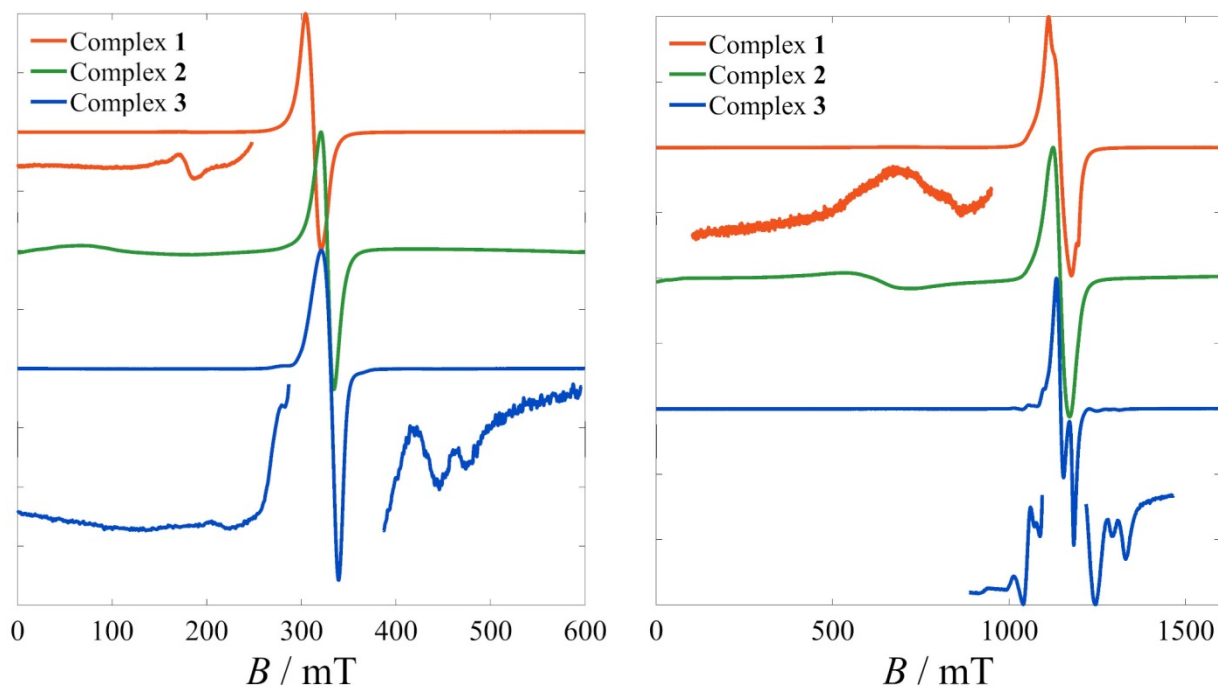


**Figure 2.** Room-temperature powder spectra of **1-3** at the X-band (left) and at the Q-band (right). Only complex **3** shows a partially resolved fine and hyperfine structure.

To better understand the magnetic properties of the three complexes, frozen solution studies were also carried out. In the X-band spectra (Figure 3, left), the hyperfine interactions of the  $A_{i\parallel}$  component were partially resolved for **1** and **3**, but not for **2**. The  $g$ -anisotropy was predictably much less resolved for all three. Q-band spectra were then collected at 5 K in the hopes of better resolving the various contributions. Indeed, at that frequency, not only was the  $g$ -anisotropy resolved, but further details emerged (Figure 3, right). First, the perpendicular component of the anisotropy  $A_{i\perp}$ , was also resolved, whereas lateral weak absorptions appeared, which were assigned to intermultiplet ( $\Delta S_T = \pm 1$ ) transitions.

These additional features of the Q-band spectra permitted their thorough analysis based on a more elaborate model. Although all three spectra demonstrated the same overall features, the most detailed analysis was carried out on the spectrum of **1** which exhibited the best S/N ratio.

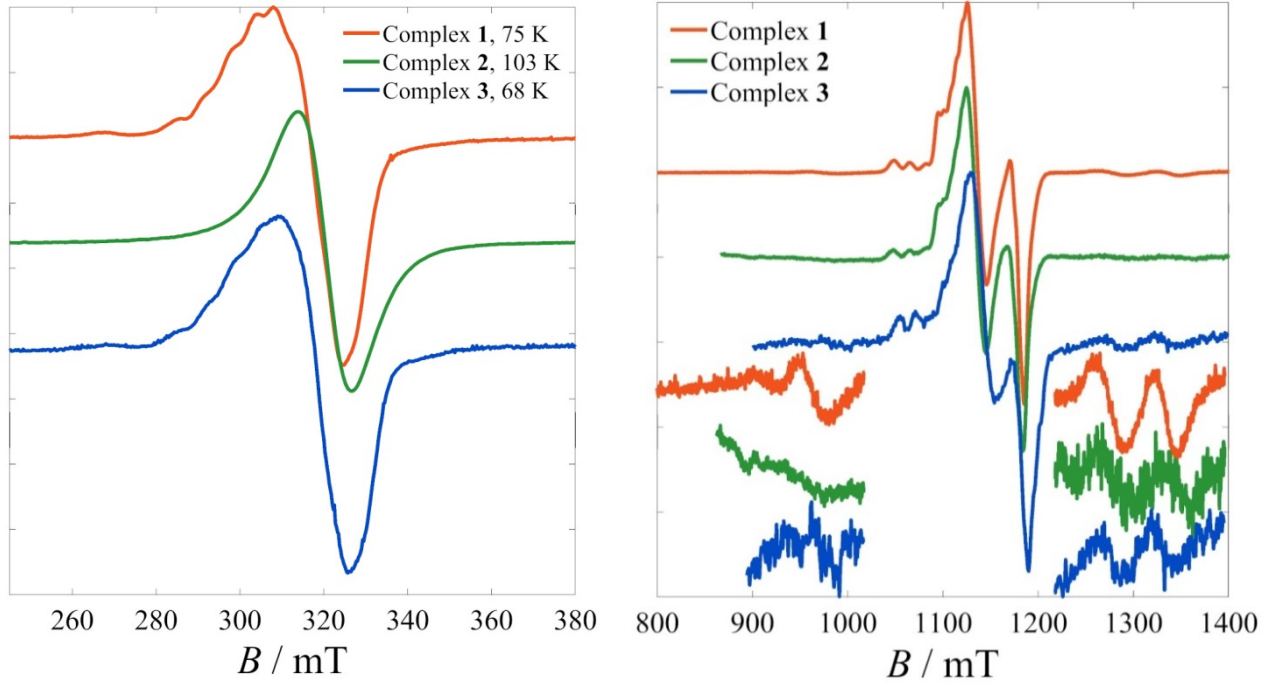


**Figure 3.** Frozen solution EPR spectra of complexes 1-3. **Left:** X-band spectra at the indicated temperatures. **Right:** Q-band spectra at 5 K.

The selected model comprised an isosceles magnetic symmetry of the isotropic (Heisenberg-Dirac-van Vleck) interactions, dipolar interactions and hyperfine interactions. The full multispin Hamiltonian was:

$$\hat{H} = J(\hat{\mathbf{S}}_1 \cdot \hat{\mathbf{S}}_2 + \hat{\mathbf{S}}_1 \cdot \hat{\mathbf{S}}_3) + J\hat{\mathbf{S}}_2 \cdot \hat{\mathbf{S}}_3 + \sum_{i,j=1}^3 \hat{\mathbf{S}}_i^T \tilde{\mathbf{D}}_{ij}^{dip} \hat{\mathbf{S}}_j + \sum_{i=1}^3 \hat{\mathbf{I}}_i^T \tilde{\mathbf{A}} \hat{\mathbf{S}}_i + \mu_B \mathbf{B}^T \sum_{i=1}^3 \tilde{\mathbf{g}}_i \hat{\mathbf{S}}_i$$

For the calculations, the fitted quantities were the average of the  $J$  and  $J'$  values and their difference, defined, respectively, as:  $J_{av} = (2J + J')/3$  and  $\Delta J = J - J'$  (whence it can be derived that  $J = (3J_{av} + \Delta J)/3$  and  $J' = (3J_{av} - 2\Delta J)/3$ ). To avoid overparametrization, the  $g$ - and  $A$ -tensor elements for the three ions were taken as identical, as were the interspin distances. The  $g$ -tensor reference frames were fixed to idealized positions based on the crystal structure, characterized by Euler angles  $\mathbf{E}_{g1} = [90^\circ, 90^\circ, -45^\circ]$ ,  $\mathbf{E}_{g2} = [30^\circ, -90^\circ, 135^\circ]$  and  $\mathbf{E}_{g3} = [-30^\circ, 90^\circ, -45^\circ]$  with respect to the molecular frame ( $\mathbf{E}_{RM} = [0, 0, 0]$ ). The  $A$ -tensors were initialized collinear to their respective  $g$ -tensors ( $\mathbf{E}_{A_i(0)} = \mathbf{E}_{g_i}$ ) and allowed to vary slightly around that position during the fitting process. To avoid overparametrization, this variation,  $\Delta_A$ , was common for all three hyperfine tensors ( $\mathbf{E}_{A_i} = \mathbf{E}_{A_i(0)} + \Delta_A$ ).

Preliminary fits were carried out with a model assuming two  $^{63}\text{Cu}$  and one  $^{65}\text{Cu}$  nucleus, which is very close to the natural abundances of the two nuclei (i.e. 69.17% and 30.83%, respectively). Simulations revealed that these were largely superimposable with the spectrum calculated assuming natural abundances on each site (Figure S1). Since, however, the simulation time rose by a factor of 8 in the latter case due to the calculation of the  $2^3$  possible isotopologues, this calculation was reserved for only the final fits and statistical analyses of the fitted variables (reported below).

The best-fit parameters to this model, along with their 95% confidence intervals thus determined, are:  $g_{\parallel} = 2.25707 \pm 0.00036$ ,  $g_{\perp} = 2.05853 \pm 0.00021$ ,  $\sigma_G = 2.31 \pm 0.80 \text{ mT}_{pp}$ ,  $\sigma_L = 2.85 \pm 0.22 \text{ mT}_{pp}$ ,  $r_{ij} = 8.22 \pm 0.11 \text{ \AA}$ ,  $J_{av} = 0.11217 \pm 0.00050 \text{ cm}^{-1}$ ,  $\Delta J = 0.0114 \pm 0.0018 \text{ cm}^{-1}$ ,  $A_{\parallel} = 502.94 \pm 8.42 \text{ MHz}$ ,  $A_{\perp} = 52.0 \pm 13.2 \text{ MHz}$ ,  $\Delta_A = [-6.4 \pm 2.5^\circ, 3.4 \pm 7.4^\circ, 28.8486 \pm 0.0005^\circ]$ . The fit is shown in Figure 4, along with the resonances calculated in the  $z$ - and  $x$ -molecular orientations of the magnetic field. The fitted tensor elements are shown in Figure 5.

The fitted transitions involve several intermultiplet ones, whose assignment is facilitated by the consideration of the low-field part of the Zeeman diagram (Figure S2). Briefly, in spin triangles, the spin-spin couplings create magnetic levels whose description can be based on the intermediate spin quantum number  $S_{23}$  (where  $\hat{\mathbf{S}}_{23} = \hat{\mathbf{S}}_2 + \hat{\mathbf{S}}_3$ ), the total spin quantum number  $S$  (where  $\hat{\mathbf{S}} = \hat{\mathbf{S}}_1 + \hat{\mathbf{S}}_{23}$ ) and the quantum number  $M_S$  of the projection of the total spin ( $= +S, +S - 1, \dots, -S$ ). In that scheme,  $S_{23}$  allows us to distinguish between the two spin doublets (e.g., for  $S_i = 1/2$  systems,  $S_{23} = 0$  or  $1$ ). However, in the present case the two doublets are too closely packed and the resonances too numerous for a clear labeling of the states to be possible with the  $|S_{23}, S, M_S\rangle$  scheme. Instead the simplified scheme  $|S, M_S\rangle$  is used in Figure 4.

Unsurprisingly, the confidence intervals indicate that the  $g$ -tensor elements are very well determined. Moreover, we also derive quite small confidence intervals for the average  $J$  value, whose magnitude closely tracks the positions of the lateral absorptions. The calculated distance is remarkably close to the crystallographically-determined

distance average of 8.29 Å (from 8.28, 8.46 and 8.12 Å distances), thus validating the hypothesis of the point-dipole model. The values of the hyperfine interactions are also quite well determined, and yield reasonable values.

One remark is in order concerning the Euler angles of the local hyperfine tensors. The first two rotation angles which, respectively, define the angular deviations from the triangle dissector and the triangle plane, are predictably small and ill-defined. However, we derive a remarkably narrow confidence interval for the third angle, which defines rotations around the local  $z$ -axes. This is interpreted more as an artifact of the covariance matrix calculation rather than as a highly certain determination of that angle. While the fits did coherently converge to a significant rotation around the local  $z$ -axes, and while these are considered as bearing true physical meaning, the narrowness of the associated confidence interval is not considered to be quantitatively reliable.

A feature that was consistently difficult to reproduce was the line width of the lateral absorptions, with calculated spectra always yielding much sharper line shapes. Inclusion of antisymmetric (Dzyaloshinskii-Moriya) interactions did not improve the agreement with the experiments. A tentative interpretation is that this line shape is associated with distributions of the exchange terms. Indeed, given the relative flexibility of the molecular scaffold, it is plausible to assume the presence of several slightly different conformations of the molecules in solution. These should be associated with slightly distributed  $J_{av}$  and  $\Delta J$  values which should contribute to this line broadening. A detailed analysis of magnetic exchange parameter distributions, would require the calculation of a series of EPR spectra, and would therefore be prohibitively time consuming due to the large Hilbert space of this problem.

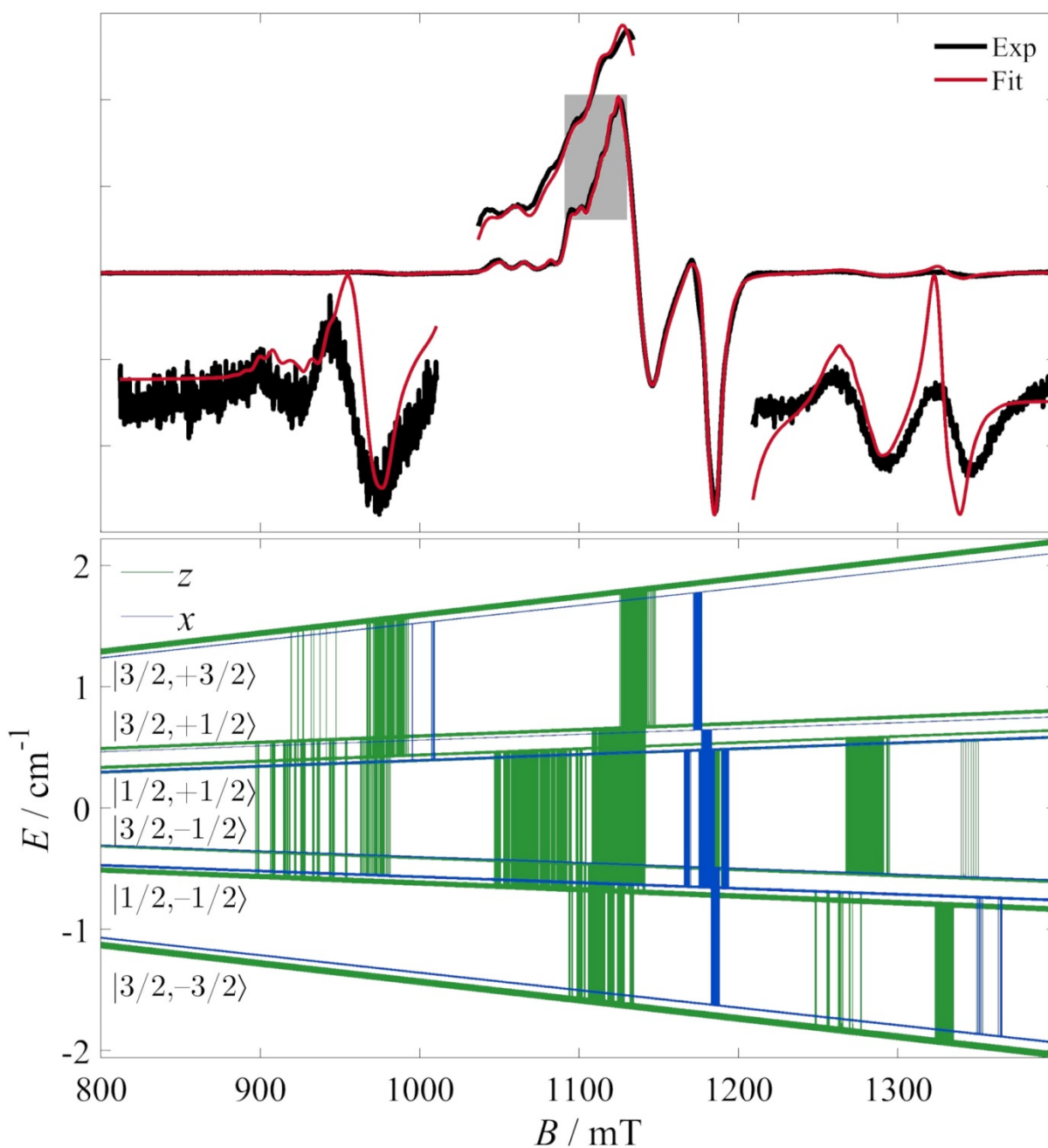


**Figure 4. Top:** CW EPR spectrum of a frozen solution (5 K) at the Q band (black lines) and best fit to the model described in the text. The bottom insets are in scale with respect to the  $x$ -axis and expanded only along the  $y$ -axis. The top inset is an expansion of the area around the  $g \sim 2.2$  region indicated by the grey rectangle. **Bottom:** Zeeman diagrams and resonances at the  $z$  (green) and  $x$  (blue) orientations in the molecular reference frame. The Zeeman diagram was calculated for an isotopologue with three  $^{63}\text{Cu}$  nuclei and assignments were facilitated by the low-field part of the diagram (Figure S2). The low- and high-field signals correspond to intermultiplet  $\Delta M_S = 1$  transitions. Low-field signals are assigned to  $|S, M_S\rangle = |1/2, -1/2\rangle \rightarrow |3/2, +1/2\rangle$  and  $|1/2, +1/2\rangle \rightarrow |3/2, +3/2\rangle$  transitions, while high-field signals to  $|3/2, -3/2\rangle \rightarrow |1/2, -1/2\rangle$  and  $|3/2, -1/2\rangle \rightarrow |1/2, +1/2\rangle$  transitions.

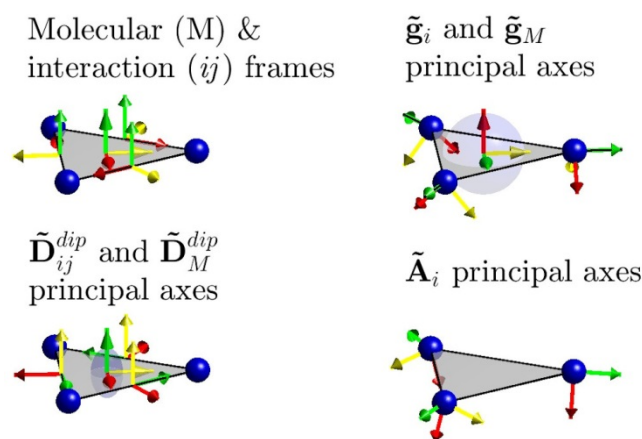


**Figure 5.** Molecular and local reference frames for interactions and tensors used in the spin Hamiltonian. The blue transparent ellipsoids indicate the anisotropy of the  $g$  and total anisotropy tensors. This latter derives purely from dipolar interactions.

To validate the model used, and justify the number of terms employed, the effect of each of these terms was demonstrated by simulations shown in Figure 6. The most salient observation is the remarkable effect of the exchange terms on the spectral appearance, both in the central and on the lateral absorptions. Simulations considering only the dipolar contributions or a simple mononuclear paramagnetic species were far from the observed spectrum.

Moreover, it was shown that the dipolar term is also necessary to reproduce the finer details of the central absorption; indeed, neglecting the dipolar terms leads to simulations of visibly lower quality, presumably from the absence of the dipolar-induced zfs in the quartet state.

The least conspicuous effect is that of the  $\Delta J$  term (Heisenberg asymmetry), also reflected on the relatively larger confidence intervals of its fitted value. Indeed, inclusion of this term mainly affects the appearance of the lateral absorptions, particularly the low-field ones. Although small, however, the role of this term is not insignificant and indicates the power of EPR spectroscopy to detect small differences of already weak exchange terms; indeed, the fitted value of  $0.0114 \text{ cm}^{-1}$  or 343 MHz, is of the order of magnitude of the hyperfine terms.

The absolute values of the principal tensor elements of the pairwise dipolar interactions at those distances were 228, 104 and 99 MHz, yielding a total zfs with  $D_{\text{dip}} = 74 \text{ MHz}$  ( $0.0025 \text{ cm}^{-1}$ ), when the local reference frames are taken into account.

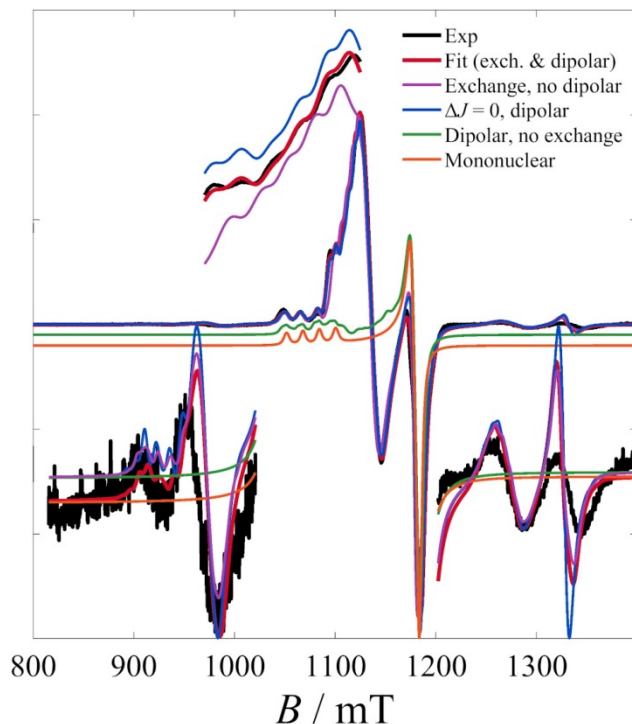


**Figure 6.** Effect of exchange terms to the calculated spectrum of **1**. Neglecting any of the electron-electron interaction terms leads to spectra of visibly worse agreement to the experimental one.

Given the relatively good quality of the Q-band spectrum of **2**, fits were attempted based on the model used for **1**, and using that best-fit solution as a point of departure. However, given the relatively poorer spectral quality, a simplification was made by considering collinear  $\mathbf{g}_i$  and  $\mathbf{A}_i$  local tensors. The best-fit parameters to this model, along with their 95% confidence intervals, are:  $g_{i\parallel} = 2.25488 \pm 0.00061$ ,  $g_{i\perp} = 2.06111 \pm 0.00025$ ,  $\sigma_G = 3.3 \pm 1.0 \text{ mT}_{\text{pp}}$ ,  $\sigma_L = 2.41 \pm 0.50 \text{ mT}_{\text{pp}}$ ,  $r_{ij} = 8.35 \pm 0.15 \text{ \AA}$ ,  $J_{av} = 0.11628 \pm 0.00073 \text{ cm}^{-1}$ ,  $\Delta J = 0.0150 \pm 0.0019 \text{ cm}^{-1}$ ,  $A_{i\parallel} = 543 \pm 14 \text{ MHz}$ ,  $A_{i\perp} = 69.6 \pm 6.4 \text{ MHz}$ .  $\Delta_A$  was fixed to  $[0, 0, 0]$ . The respective calculated spectrum is shown in Figure 7 (left).

Finally, similar fits were attempted for the powder room-temperature spectra of **3** (Figure 7, right), whose fine structure made such fits feasible. It is suggested that the observation of this fine structure is probably due to the larger intermolecular separations in the solid state, which reduce dipolar broadenings. The previously determined parameters proved to be a suitable starting point for the fits to this spectrum. However, the predictably poorer resolution of the hyperfine interactions, as well as some additional features in the lateral (intermultiplet) absorptions, add some uncertainty to these fits. Accordingly, these are treated as simulations and the results are given without a detailed statistical treatment. These are:  $g_{i\parallel} = 2.230$ ,  $g_{i\perp} = 2.061$ ,  $\sigma_G = 3.31 \text{ mT}_{\text{pp}}$ ,  $\sigma_L = 3.85 \text{ mT}_{\text{pp}}$ ,  $r_{ij} = 8.22 \text{ \AA}$ ,  $J_{av} = 0.078 \text{ cm}^{-1}$ ,  $\Delta J = 0.011 \text{ cm}^{-1}$ ,  $A_{i\parallel} = 540.0 \text{ MHz}$ ,  $A_{i\perp} = 48.0 \text{ MHz}$ .  $\Delta_A$  was fixed to  $[0, 0, 0]$ .

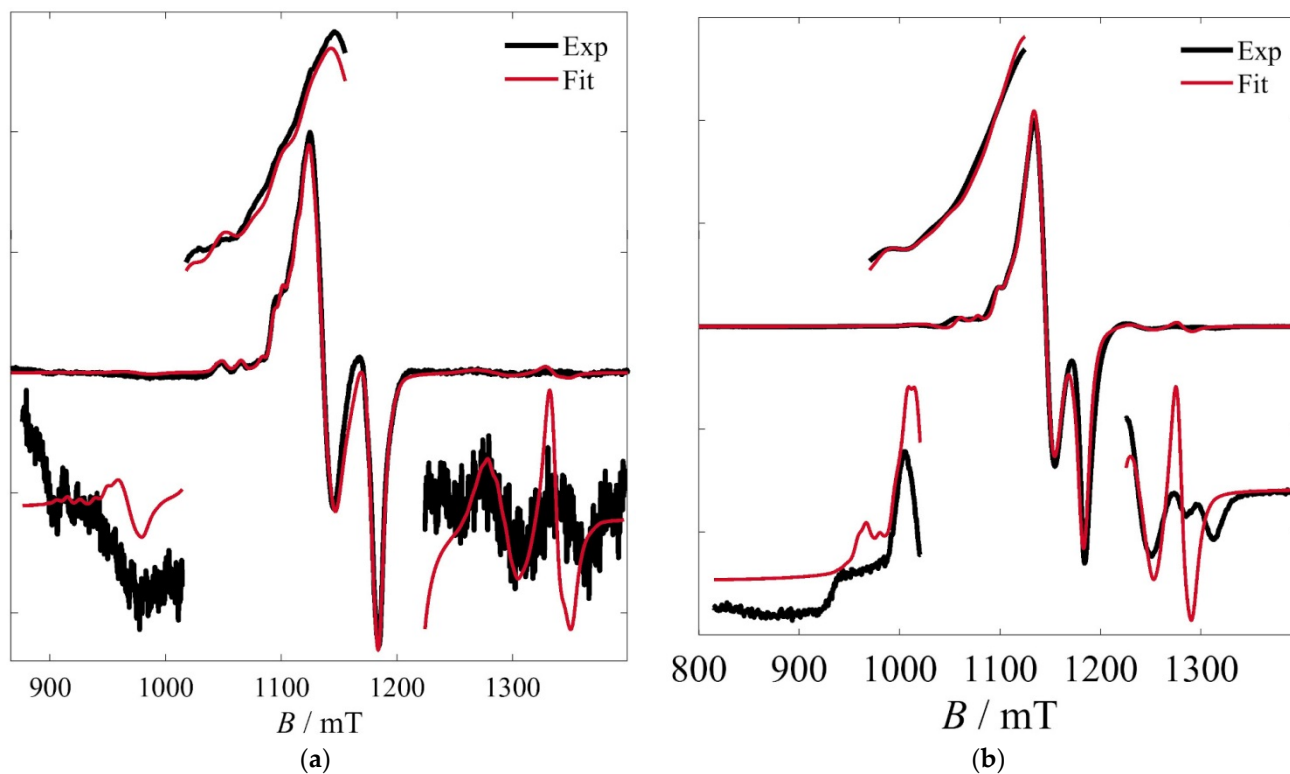


**Figure 7.** **Left:** Q-band spectrum from a frozen solution of **2** at 5 K and best fits according to the model and parameters described in the text. **Right:** Q-band spectrum from a powdered sample of **3** at 295 K and simulation according to the model and parameters described in the text.

### 3. Discussion and comparative analyses

This work demonstrates that EPR spectroscopy can be successfully used to address weak spin-spin interactions in relatively complicated polynuclear systems, thus providing an important complement to magnetometric studies. Indeed, the detailed EPR study of **1-3** allowed the estimation of very weak exchange interactions as well as dipolar couplings, to a level of confidence practically unattainable with magnetic susceptometry experiments. Notably, a single EPR experiment for each complex provided sufficient information for the determination of those interactions in parallel to hyperfine ones.

As far as the specific complexes of this study are concerned, these were shown to exhibit a close agreement in their magnetic properties (Table 1), in accordance to their very similar molecular structures. Regarding the exchange and hyperfine interactions, the rationalization of their precise magnitudes requires the use of theoretical models, which is beyond the scope of this work. However, regarding the larger line widths of **3**, these may plausibly be attributed to remaining intermolecular dipolar interactions in the solid state which give rise to smaller but non-negligible dipolar broadenings.

**Table 1.** Spin-Hamiltonian parameters of **1-3** as determined from fits to frozen solution (**1, 2**) and powder (**3**) Q-band EPR spectra.

	<b>1</b>	<b>2</b>	<b>3</b>
$g_{\parallel}$	2.25707±0.00036	2.25488±0.00061	2.230
$g_{i\perp}$	2.05853±0.00021	2.06111±0.00025	2.061
$\sigma_G / \sigma_L$ (mT <sub>pp</sub> )	2.31±0.80 / 2.85±0.22	3.3±1.0 / 2.41±0.50	3.3 / 3.9
$r_{ij}$ (Å)	8.22±0.11	8.35±0.15	8.22
$J_{av}$ (cm <sup>-1</sup> )	0.11217±0.00050	0.11628±0.00073	0.078
$\Delta J$ (cm <sup>-1</sup> )	0.0114±0.0018	0.0150±0.0019	0.011
$A_{\parallel}$ (MHz)	502.94±8.42	543±14	540
$A_{i\perp}$ (MHz)	52.0±13.	69.6±6.4	48
$\Delta_A$ (°)	[-6.4±2.5, 3.4±7.4, 28.8486±0.0005]	[0, 0, 0]	[0, 0, 0]

It should be noted that similar systems have been studied in the past, using EPR spectroscopy at even higher fields like in the case of Cu<sup>II</sup><sub>3</sub> triangles encapsulated in polyoxometallates. In particular, powder W-band EPR spectra of K<sub>9</sub>Na[Cu<sub>3</sub>(H<sub>2</sub>O)<sub>3</sub>( $\alpha$ -TeW<sub>9</sub>O<sub>33</sub>)<sub>2</sub>] $\cdot$ 16H<sub>2</sub>O [17] and Na<sub>9</sub>[Cu<sub>3</sub>Na<sub>3</sub>(H<sub>2</sub>O)<sub>9</sub>( $\alpha$ -AsW<sub>9</sub>O<sub>33</sub>)<sub>2</sub>] $\cdot$ 26H<sub>2</sub>O [18] were simulated by a giant spin approach, with the exchange interactions determined independently by variable-temperature magnetic susceptometry. Subsequently, single-crystal studies of the latter complex were complemented by pulsed field-sweep experiments for the same purpose [19,20]. Despite the clear presence of intermultiplet resonances in these latter spectra, these resonances were not simulated for the determination of exchange interactions.

Of relevance are also studies of the extensively explored polyoxovanadate system K<sub>6</sub>[V<sub>15</sub>As<sub>6</sub>O<sub>42</sub>(H<sub>2</sub>O)] $\cdot$ 8H<sub>2</sub>O, or “V<sub>15</sub>”, whose precise determination of the spin-spin interactions has been a contentious issue. The metallic core of the molecule can be considered as three-layered, i.e. {V<sub>6</sub>-V<sub>3</sub>-V<sub>6</sub>}, with the top and bottom “V<sub>6</sub>” layers exhibiting strong antiferromagnetic interactions which quench their magnetizations. Thus the low-temperature magnetic properties of the molecule are usually treated as stemming from the weakly coupled triangular “V<sub>3</sub>” layer.[21] It is of note that while extensive studies have been conducted employing an arsenal of techniques, such as various types of magnetometry [22,23], EPR at various frequencies [24], inelastic neutron scattering [25], heat capacity [26] and NMR spectroscopy [27], there still remain ambiguities around the precise nature of the spin-spin interactions of this molecule. Application of the models described in this work should complement our understanding of this question.

#### 4. Conclusions

Overall, the development of detailed models integrating exchange and dipolar interactions, can be very useful for the determination of very weak such interactions, and allow the full unlocking of the information contained in EPR spectra. Indeed, the broad availability of EPR simulation tools, such as *Easyspin* [28] or *Phi* [29], that consider arbitrary multispin Hamiltonians, makes the development of such models a tractable task, albeit not a routine one. Moreover, the increases in performance of computer processors over the past years have brought the unavoidable computational overhead of such models within the reach of even personal computers.

The combination of the above can allow the detailed description of the magnetic spectra of a large number of weakly interacting molecular or biological polynuclear systems, currently beyond the reach of magnetometric techniques. On the one hand, the new information gleaned from detailed treatment of EPR spectra should be particularly useful in refining first-principles theoretical models attempting to determine such interactions from known molecular structures; accurate determinations of weak exchange, would push these models to their limits and reveal avenues for their improvement. On the other hand this information would be helpful in structure elucidation of biological systems from their EPR signatures; structures of metalloenzyme active sites containing polymetallic weakly-coupled magnetic cores could be deduced in the absence of high-resolution crystal data.

In conclusion, the implementation of such detailed models should complement the understanding of multispin molecular or biological systems, even using powder/frozen solution EPR spectra.

#### 5. Experimental

##### *Syntheses*

*Dipyatriz.* The synthesis was carried out according to the process described in the literature.[30] Recrystallization of 4.4 g of the crude product was carried out by dissolving in 120 mL of warm CH<sub>2</sub>Cl<sub>2</sub> and precipitating by the addition of *n*-hexane. After filtration and drying, the yield was 2.2 g of pure ligand.

*Complex I.* This was synthesized according to the process described in the literature using a stoichiometric reaction of the starting materials.[13] The blue powder that precipitated analyzed as **1** $\cdot$ 4.6H<sub>2</sub>O (0.903 g, 52% on ligand basis or metal basis) and slow evaporation of the filtrate yielded single crystals whose unit cell determination matched the published structure.

---

*Complex 2.* This was first reported[13] as an accidental product and its synthesis has now been rationalized. In particular, solid dipyratiz (0.214 g, 0.360 mmol) was added to a MeOH solution (110 mL) containing  $\text{CuCl}_2 \cdot 2\text{H}_2\text{O}$  (0.0460 g, 0.270 mmol) and  $\text{Cu}(\text{ClO}_4)_2 \cdot 6\text{H}_2\text{O}$  (0.100 g, 0.270 mmol). In the absence of full dissolution of the ligand, 35 mL of MeCN were added to the mixture, causing full dissolution in a few minutes and a deep blue solution. In three days, good parallelepiped crystals had formed, whose unit cell determination confirmed their identity. The yield was 37.3 mg (9%).

*Complex 3.* This was synthesized according to the reported procedure [14].

#### *EPR spectroscopy*

CW EPR spectra were collected on an EMXplus spectrometer controlled by the Bruker Xenon software, with the magnetic applied by a Bruker BE25 electromagnet using a Bruker ER082(155/45)Z power supply.

For X-band experiments, the spectrometer was fitted with an EMX microX bridge and a Bruker ER4122SHQE cavity operating in the  $\text{TE}_{011}$  mode. Low-temperature experiments were carried out using an ESR900 dynamic continuous flow cryostat and the temperature was regulated with an Oxford ITC4 servocontrol. For Q-band spectra, the spectrometer was fitted with an EMX premiumQ microwave bridge and an ER5106QTW microwave resonator operating in the  $\text{TE}_{012}$  mode. For low-temperature experiments the resonator was fitted in an Oxford CF935 dynamic continuous flow cryostat and the temperature was regulated with an Oxford ITC503 servocontrol.

Fits to the EPR data and simulations were carried out with *Easyspin* v. 6.0 using custom-made routines.[28]

The EPR solutions of **1** (0.54 mM in MeOH for the X-band experiments and 1.34 mM in MeOH/MeCN 50:50 for the Q-band experiments), **2** (0.84 mM in MeCN) and **3** (0.40 mM in MeCN) were deoxygenated with freeze-pump-thaw cycles, flame-sealed under a helium atmosphere in the EPR tubes and stored in liquid nitrogen.

**Acknowledgments:** This project has received funding from the European Union's Horizon 2020 research and innovation programme under the Marie Skłodowska-Curie grant agreement No 746060 (project "CHIRALQUBIT"). I particularly wish to thank Dr. Romain Ruppert for the synthesis of the ligand.

## References

1. Boudalis, A. Half-Integer Spin Triangles: Old Dogs, New Tricks. *Chemistry – A European Journal* **2020**, doi:10.1002/chem.202004919.
2. Boudalis, A.K.; Robert, J.; Turek, P. First Demonstration of Magnetolectric Coupling in a Polynuclear Molecular Nanomagnet: Single-Crystal EPR Studies of  $[\text{Fe}_3\text{O}(\text{O}_2\text{CPh})_6(\text{Py})_3]\text{ClO}_4\cdot\text{py}$  under Static Electric Fields. *Chem. Eur. J.* **2018**, *24*, 14896–14900, doi:10.1002/chem.201803038.
3. Robert, J.; Parizel, N.; Turek, P.; Boudalis, A.K. Polyanisotropic Magnetolectric Coupling in an Electrically Controlled Molecular Spin Qubit. *Journal of the American Chemical Society* **2019**, *141*, 19765–19775, doi:10.1021/jacs.9b09101.
4. Liu, J.; Mrozek, J.; Myers, W.K.; Timco, G.A.; Winpenny, R.E.P.; Kintzel, B.; Plass, W.; Ardavan, A. Electric Field Control of Spins in Molecular Magnets. *Physical Review Letters* **2019**, *122*, 037202, doi:10.1103/PhysRevLett.122.037202.
5. Kintzel, B.; Fittipaldi, M.; Böhme, M.; Cini, A.; Tesi, L.; Buchholz, A.; Sessoli, R.; Plass, W. Spin–Electric Coupling in a Cobalt(II)-Based Spin Triangle Revealed by Electric-Field-Modulated Electron Spin Resonance Spectroscopy. *Angew Chem Int Ed* **2021**, *60*, 8832–8838, doi:10.1002/anie.202017116.
6. Lewkowicz, M.; Adams, J.; Sullivan, N.S.; Wang, P.; Shatruk, M.; Zapf, V.; Arvij, A.S. Direct Observation of Electric Field-Induced Magnetism in a Molecular Magnet. *Sci Rep* **2023**, *13*, 2769, doi:10.1038/s41598-023-29840-1.
7. Trif, M.; Troiani, F.; Stepanenko, D.; Loss, D. Spin-Electric Coupling in Molecular Magnets. *Physical Review Letters* **2008**, *101*, 217201, doi:10.1103/PhysRevLett.101.217201.
8. Trif, M.; Troiani, F.; Stepanenko, D.; Loss, D. Spin Electric Effects in Molecular Antiferromagnets. *Physical Review B* **2010**, *82*, 045429, doi:10.1103/PhysRevB.82.045429.
9. Troiani, F.; Stepanenko, D.; Loss, D. Hyperfine-Induced Decoherence in Triangular Spin-Cluster Qubits. *Physical Review B* **2012**, *86*, 161409(R), doi:10.1103/PhysRevB.86.161409.
10. Stepanenko, D.; Trif, M.; Tsypliyatyev, O.; Loss, D. Field-Dependent Superradiant Quantum Phase Transition of Molecular Magnets in Microwave Cavities. *Semiconductor Science and Technology* **2016**, *31*, 094003, doi:10.1088/0268-1242/31/9/094003.
11. Bencini, A.; Gatteschi, D.; Bencini, A. *EPR of Exchange Coupled Systems*; Dover ed.; Dover Publications, Inc: Mineola, N.Y., 2012; ISBN 978-0-486-48854-7.
12. Mathivathanan, L.; Rogez, G.; Ben Amor, N.; Robert, V.; Raptis, R.G.; Boudalis, A.K. Origin of Ferromagnetism and Magnetic Anisotropy in a Family of Copper(II) Triangles. *Chem. Eur. J.* **2020**, *26*, 12769–12784, doi:10.1002/chem.202001028.
13. Barrios, L.A.; Aromí, G.; Frontera, A.; Quiñero, D.; Deyà, P.M.; Gamez, P.; Roubeau, O.; Shotton, E.J.; Teat, S.J. Coordination Complexes Exhibiting Anion- $\pi$  Interactions: Synthesis, Structure, and Theoretical Studies. *Inorganic Chemistry* **2008**, *47*, 5873–5881, doi:10.1021/ic800215r.
14. Yuste, C.; Cañadillas-Delgado, L.; Labrador, A.; Delgado, F.S.; Ruiz-Pérez, C.; Lloret, F.; Julve, M. Low-Dimensional Copper(II) Complexes with the Trinucleating Ligand 2,4,6-Tris(Di-2-Pyridylamine)-1,3,5-Triazine: Synthesis, Crystal Structures, and Magnetic Properties. *Inorganic Chemistry* **2009**, *48*, 6630–6640, doi:10.1021/ic900599g.
15. Demeshko, S.; Leibel, G.; Dechert, S.; Meyer, F. 1,3,5-Triazine-Based Tricopper(I) Complexes: Structure and Magnetic Properties of Threefold-Symmetric Building Blocks. *Dalton Trans.* **2004**, 3782, doi:10.1039/b407598f.
16. Chen, J.; Wang, X.; Shao, Y.; Zhu, J.; Zhu, Y.; Li, Y.; Xu, Q.; Guo, Z. A Trinuclear Copper(II) Complex of 2,4,6-Tris(Di-2-Pyridylamine)-1,3,5-Triazine Shows Prominent DNA Cleavage Activity. *Inorg. Chem.* **2007**, *46*, 3306–3312, doi:10.1021/ic0614162.
17. Stowe, A.C.; Nellutla, S.; Dalal, N.S.; Kortz, U. Magnetic Properties of Lone-Pair-Containing, Sandwich-Type Polyoxoanions: A Detailed Study of the Heteroatomic Effect. *European Journal of Inorganic Chemistry* **2004**, *2004*, 3792–3797, doi:10.1002/ejic.200400234.
18. Kortz, U.; Nellutla, S.; Stowe, A.C.; Dalal, N.S.; van Tol, J.; Bassil, B.S. Structure and Magnetism of the Tetra-Copper(II)-Substituted Heteropolyanion  $[\text{Cu}_4\text{K}_2(\text{H}_2\text{O})_8(\alpha\text{-AsW}_9\text{O}_{33})_2]^{8-}$ . *Inorganic Chemistry* **2004**, *43*, 144–154, doi:10.1021/ic034697b.
19. Choi, K.-Y.; Matsuda, Y.H.; Nojiri, H.; Kortz, U.; Hussain, F.; Stowe, A.C.; Ramsey, C.; Dalal, N.S. Observation of a Half Step Magnetization in the  $\{\text{Cu}_3\}$ -Type Triangular Spin Ring. *Phys. Rev. Lett.* **2006**, *96*, 107202, doi:10.1103/PhysRevLett.96.107202.
20. Choi, K.-Y.; Dalal, N.S.; Reyes, A.P.; Kuhns, P.L.; Matsuda, Y.H.; Nojiri, H.; Mal, S.S.; Kortz, U. Pulsed-Field Magnetization, Electron Spin Resonance, and Nuclear Spin-Lattice Relaxation in the  $\{\text{Cu}_3\}$  Spin Triangle. *Phys. Rev. B* **2008**, *77*, 024406, doi:10.1103/PhysRevB.77.024406.
21. Gatteschi, D.; Pardi, L.; Barra, A.L.; Müller, A.; Döring, J. Layered Magnetic Structure of a Metal Cluster Ion. *Nature* **1991**, *354*, 463–465, doi:10.1038/354463a0.
22. Tarantul, A.; Tsukerbat, B.; Müller, A. High-Field Magnetization of  $V_{15}$  Cluster at Ultra-Low Temperatures: Importance of Antisymmetric Exchange and Its Precise Estimation. *Chemical Physics Letters* **2006**, *428*, 361–366, doi:10.1016/j.cplett.2006.07.025.
23. Tarantul, A.; Tsukerbat, B.; Müller, A. Static Magnetization of  $V_{15}$  Cluster at Ultra-Low Temperatures: Precise Estimation of Antisymmetric Exchange. *Inorg. Chem.* **2007**, *46*, 161–169, doi:10.1021/ic061394j.
24. Vongtragool, S.; Gorshunov, B.; Mukhin, A.A.; van Slageren, J.; Dressel, M.; Müller, A. High-Frequency Magnetic Spectroscopy on the Molecular Magnetic Cluster  $V_{15}$ . *Phys. Chem. Chem. Phys.* **2003**, *5*, 2778–2782, doi:10.1039/B302244G.
25. Chaboussant, G.; Ochsenbein, S.T.; Sieber, A.; Güdel, H.-U.; Mutka, H.; Müller, A.; Barbara, B. Mechanism of Ground-State Selection in the Frustrated Molecular Spin Cluster  $V_{15}$ . *EPL* **2004**, *66*, 423–429, doi:10.1209/epl/i2004-10008-x.
26. Fu, Z.; Xiao, Y.; Su, Y.; Zheng, Y.; Kögerler, P.; Brückel, T. Low-Lying Magnetic Excitations and Magnetocaloric Effect of Molecular Magnet  $\text{K}_6[\text{V}_{15}\text{As}_6\text{O}_{42}(\text{H}_2\text{O})] \cdot 8\text{H}_2\text{O}$ . *EPL* **2015**, *112*, 27003, doi:10.1209/0295-5075/112/27003.
27. Furukawa, Y.; Nishisaka, Y.; Kumagai, K.; Kögerler, P.; Borsa, F. Local Spin Moment Configuration in the Frustrated  $s = 1/2$  Heisenberg Triangular Antiferromagnet  $V_{15}$  Determined by NMR. *Phys. Rev. B* **2007**, *75*, 220402, doi:10.1103/PhysRevB.75.220402.
28. Stoll, S.; Schweiger, A. EasySpin, a Comprehensive Software Package for Spectral Simulation and Analysis in EPR. *Journal of Magnetic Resonance* **2006**, *178*, 42–55, doi:10.1016/j.jmr.2005.08.013.
29. Chilton, N.F.; Anderson, R.P.; Turner, L.D.; Soncini, A.; Murray, K.S. PHI: A Powerful New Program for the Analysis of Anisotropic Monomeric and Exchange-Coupled Polynuclear *d*- and *f*-Block Complexes. *Journal of Computational Chemistry* **2013**, *34*, 1164–1175, doi:10.1002/jcc.23234.
30. Pang, J.; Tao, Y.; Freiberg, S.; Yang, X.-P.; D'Iorio, M.; Wang, S. Syntheses, Structures, and Electroluminescence of New Blue Luminescent Star-Shaped Compounds Based on 1,3,5-Triazine and 1,3,5-Trisubstituted Benzene. *J. Mater. Chem.* **2002**, *12*, 206–212, doi:10.1039/b105422h.

